Selected Papers from the 9th Scandinavian Conference on Image Analysis

THEORY AND APPLICATIONS OF IMAGE ANALYSIS II

editor

Gunilla Borgefors

Centre for Image Analysis, SUAS
Uppsala, Sweden

World Scientific
Singapore • New Jersey • London • Hong Kong

Published by

World Scientific Publishing Co. Pte. Ltd.

P O Box 128, Farrer Road, Singapore 9128

USA office: Suite 1B, 1060 Main Street, River Edge, NJ 07661

UK office: 57 Shelton Street, Covent Garden, London WC2H 9HE

British Library Cataloguing-in-Publication Data
A catalogue record for this book is available from the British Library.

THEORY AND APPLICATIONS OF IMAGE ANALYSIS II
Selected Papers from the 9th Scandinavian Conference on Image Analysis

ISBN: 981-02-2448-6

This book is printed on acid-free paper.

Printed in Singapore by Uto-Print

INTRODUCTION

The 31 papers presented in this volume were selected among the presentations at *The 9th Scandinavian Conference on Image Analysis,* which was held in Uppsala, Sweden, in June 1995. All papers have been considerably expanded and updated compared to the conference papers, to provide a maximum amount of information to the reader.

Two purposes guided the selection of the papers. The first, and most important one, was to present the best, most interesting and novel conference papers. The second one was to arrange the selected papers in coherent groups, giving different insights on related topics. The broad coverage of the conference made it impossible to represent all its subject areas. However, this selection includes most of the papers given the highest recommendation by the conference reviewers.

The papers are divided in seven sections. The first two discusses very basic image features; edges and texture, respectively. The third section concerns the problem of recovering depth information and the fourth deals with scene analysis. The fifth section presents various methods of recovering 3D motion. These five sections contain rather theoretical papers. The last two sections are more application oriented, concentrating on biomedical and industrial applications, which are two of the most active areas. The papers are briefly introduced below.

EDGES AND CURVES remain fundamental concepts in image analysis. Edge segments must be detected, linked to meaningful curves, and classified.

In *"Modelling and testing the stability of edge segments: Length and orientation"* a model is derived for the variance in length and orientation of edge segments. The model gives an insight into how the original uncertainties in extracted features due to noise influences the final edge segments.

Probabilistic Hough transforms for curve detection have emerged in recent years. In *"Connective randomized Hough transform (CRHT)"* the Randomized Hough Transform is extended to improve the performance in noisy, complex images. The CRHT combines high speed with low memory usage.

Edge segments must usually be combined into differently shaped curves, not only straight lines. In *"From edgels to parametric curves"* a robust algorithm for achieving this, for both dense and sparse edge data, is presented. Different types of parametric curves are handled concurrently.

If the scene is 3D, then the edge analysis should reflect this fact. In *"Segmentation and classification of edges using minimum description length approximation and complementary junction cues"* junction candidates and tentative break points are generated in a pre-processing step. An MDL approximation then classifies the 3D edge segments.

The last paper on edges, *"An edge labelling scheme for polyhedra in incomplete range images,"* combines grey level images with coded light range images. Edges of polyhedra are classified as jump, convex, concave, or non-geometric (shadow) edges using cues from both images.

TEXTURE is another fundamental concept in image analysis. The search for new, discriminating texture measures continues, as does the investigation of the segmentation power of various approaches.

Several new texture measures are defined in *"Texture analysis using grey level gap length matrix."* The grey level gap length matrix is a complement to the grey level run length matrix. The measures provide efficient texture classification, periodicity detection and image granulometry.

Fractal dimension can be considered as a texture measure. In *"Fractal dimension and lacunarity estimated by sequential 1D polygonization of 2D images"* a new method for estimating local fractal dimension is introduced, together with two new lacunarity measures.

Sparse texture presents additional challenges. In *"Texture gradients in sparse texture fields"* some of these are addressed. Texture gradients are estimated and segmentation is performed, using local phase and normalised differential convolution. Regions of significance in combination with local frequency yield confidence measures.

Local phase is central also in *"Texture boundary tracking with Gabor phase."* In contrast to classic methods, the authors concentrate on Gabor phase rather than magnitude. For computational convenience, the phase gradient, rather than the phase itself, is used when tracking texture boundaries.

In computer vision **DEPTH AND STEREO** information must be extracted using robust methods. The number of views and the amount of a priory information varies in the following papers.

Camera calibration is usually necessary when recovering depth. However, *"Reconstruction and prediction from three images of uncalibrated cameras"* describes an algorithm for identifying the 3D locations of a number of points without camera calibration.

If some information is added, two views are sufficient. In *"Binocular dense depth reconstruction using isotropy constraint"* two calibrated perspective views are used to make a direct metric reconstruction of the scene. It uses assumptions of rotational invariance of 3D space and camera projection models.

Specular objects are usually considered difficult. In *"Estimating circular shape using binocular stereopsis and two-source active illumination,"* specular reflections are used as the most important shape cue for recovering CAD compatible range data. The method uses two views and two alternate light sources.

The last paper in this group, *"A vision sensor for building 3-D models of structured environment,"* uses a single, mobile camera. Edges and combinations of edges are tracked, using Kalman filters, to reconstruct the environment. The uncertainties are carefully modelled.

In **SCENE ANALYSIS** objects are localised and either identified or modelled in 3D space. Object models range from the general to the specific.

In *"Reconstruction of generalized cylinders under full perspective projection by monocular vision"* the objects are generalised cylinders with a known, constant, circular cross-section. It is shown that this class is restrictive enough to permit object reconstruction from a single perspective view.

The next paper, *"The use of silhouettes in 3D scene recognition and pose estimation,"* extends the object class to solid "industrial" objects. The known objects are identified and localised in non-occluded and occluded scenes using stereo cameras. The method combines the stereo images, using object silhouettes, and a derived structure containing 3D information.

There is no restriction on the objects in *"Segmentation and recognition of 3D objects using parametric eigenspace representation."* Instead, a learning set of images of the object in varying pose and size is used. The image set is represented by a manifold in the compressed subspace spanned by eigenvectors of the image set. This representation is used to spot the object in complex images.

The remaining paper in this group, *"An interest operator based on perceptual grouping,"* is rather different from the previous ones. Complex structures, such as bridges in aerial images, are detected by an interest operator. The interest level of a region increases exponentially, as more basic features possibly belonging to the structure are detected.

3D MOTION is investigated in the last group of theoretically oriented papers. In the first papers the problem is to identify and analyse areas where motion occurs, while the subsequent ones present object tracers.

Optical flow is a well-known concept, but there are still problems estimating higher order properties of flow fields. In *"Direct estimation of first order optic flow"* curl, divergence, and deformation are estimated. The estimations are performed in a group theoretic framework and based on invariances of the Fourier transform.

In *"A model of the MRF with three observation sources for obtaining the masks of moving objects"* the areas where motion occurs in image sequences are detected. Three features are used at each pixel: difference in brightness, the brightness itself, and the value of the motion mask. The method is based on Markov Random Field modelling.

Markov Random Field theory is also used in *"Detection of small and slow moving objects observed by a mobile camera."* First, the motion is compensated using a 2D quadratic motion model. Observations are derived from temporal filtering operations. The moving objects are then detected by solving a binary labelling problem.

A completely different way of constructing an object tracer is presented in *"Object tracking based on the orientation tensor concept."* The 3D orientation tensor (two spatial dimensions plus time) and its eigenvalues and eigenvectors are used. Object size and position are estimated, while camera motion is compensated.

BIOMEDICAL APPLICATIONS have become one of the most active areas for utilisation of image analysis. New, challenging sensors are becoming standard equipment in research laboratories and hospitals. The papers are ordered from the general to the more specific.

The first paper, *"Creating and comparing sets of principal component images,"* addresses the problem of analysing a set of highly dependent images, such as a time series. The system presented is set in an interactive environment. Examples using MR and PET images are given.

A quite general approach to segmentation is found in *"General-purpose soft tissue segmentation from medical images."* It is based on interactive deformable contours (also known as "snakes"). The methods are demonstrated on a wide variety of imagery. Examples include segmentation of nerve cells in optical microscopy and of brain structures in MR data.

The title *"Measuring shape and motion of white blood cells from sequences of fluorescence microscopy images"* is self-explanatory. To identify the cells in the sequence, a two-pass spatio-temporal segmentation is used. After segmentation, shape features are estimated and cell motion is measured from these features.

In *"Mapping the human retina"* the task is to map macular degeneration of the retina for diagnosis and subsequent treatment. The image source is a scanning laser opthalmoscope. A number of radiometrically different images are obtained. They are matched using a new technique based on symbolic information. Finally, information on anatomical features and pathological changes is fused to a map.

Ultrasonic images are notoriously noisy. In *"Restoration of radial optical flows in echocardiographic sequences"* a new method for estimating the motion of the left ventricle of the heart is presented. It is based on a 1D version of the optical flow technique. The system is a useful tool for characterisation of ischemia in the cardiac function.

In *"Initial results of automated melanoma recognition"* images obtained from epiluminescence microscopy are used for early skin cancer recognition. A set of both radiometric and shape features is used to classify skin lesions. The features are merged using a Karhunen-Loeve transform and minimum distance classification.

INDUSTRIAL APPLICATIONS using advanced rather than simplistic methods are also becoming more common, as image analysis grows towards maturity. As proven by two of the selected papers, colour often carries necessary information.

A system for high speed pixel-wise spectral classification is presented in *"Near-sensor real time spectral classification for industrial applications."* The system is based on a line imaging spectrograph and a smart image sensor. The implementation is "near-sensor," using variable exposure times and analogue summation of pixel data.

The economically important problem of automatic lumber grading is treated in *"A color vision approach for grading lumber."* The computational solutions using colour images are shown to be simpler than with grey-level images, compensating for the larger data set and the higher cost of the imaging system.

In *"Automatic fruit blemish detection"* colour is also important, as blemishes appear as discoloured patches. The blemishes must be discriminated from the concave stalk and calyx areas. This is achieved using range data from structured light images. A neural network has been trained to classify detected patches, based on the intensity and range images.

The last paper, *"On edge density for automatic size inspection,"* treats a problem from the quarry industry. The task is to supervise the average size of stones on a high-speed conveyor belt. The solution is to use moment-based edge density measures and show that they give good estimates on average particle size.

Gunilla Borgefors

CONTENTS

Introduction ix

Edges and Curves

Modelling and Testing the Stability of Edge Segments: Length and Orientation 1
C. B. Madsen and H. I. Christensen

Connective Randomized Hough Transform (CRHT) 15
H. Kälviäinen and P. Hirvonen

From Edgels to Parametric Curves 27
M. Stricker and A. Leonardis

Segmentation and Classification of Edges Using Minimum Description Length Approximation and Complementary Junction Cues 39
T. Lindeberg and M.-X. Li

An Edge Labeling Scheme for Polyhedra in Incomplete Range Images 53
R. Robmann and H. Bunke

Texture

Texture Analysis Using Gray Level Gap Length Matrix 65
X.-L. Wang, F. Albregtsen and B. Foyn

Fractal Dimension and Lacunarity Estimated by Sequential 1D Polygonization of 2D Images 79
F. Albregtsen and B. Nielsen

Texture Gradients in Sparse Texture Fields 89
M. Ulvklo, G. Granlund and H. Knutsson

Texture Boundary Tracking with Gabor Phase 101
S. Fisher and J. Bigün

Depth and Stereo

Reconstruction and Prediction from Three Images of Uncalibrated Cameras 113
A. Heyden

Binocular Dense Depth Reconstruction Using Isotropy Constraint 127
M. Nielsen and R. Deriche

Estimating Circular Shape Using Binocular Stereopsis and Two-Source Active Illumination 141
P. Kierkegaard

A Vision Sensor for Building 3-D Models of Structured Environment 155
T. Repo and O. Silvén

Scene Analysis

Reconstruction of Generalized Cylinders Under Full Perspective Projection by Monocular Vision 169
P. Sayd, M. Dhome and J.-M. Lavest

The Use of Silhouettes in 3D Scene Recognition and Pose Estimation 183
R. M. Hoogeveen and M. J. Korsten

Segmentation and Recognition of 3D Objects Using Parametric Eigenspace Representation 197
H. Murase and S. K. Nayar

An Interest Operator Based on Perceptual Grouping 211
H. S. Dabis, P. L. Palmer and J. Kittler

3D Motion

Direct Estimation of First Order Optic Flow 225
J. Sporring and M. Nielsen

A Model of the MRF With Three Observation Sources for Obtaining the Masks of Moving Objects 239
A. Kuriański and M. Nieniewski

Detection of Small and Slow Moving Objects Observed by a Mobile Camera 253
C. Hennebert, V. Rebuffel and P. Bouthemy

Object Tracking Based on the Orientation Tensor Concept 267
J. Karlholm, C.-J. Westelius, C.-F. Westin and H. Knutsson

Biomedical Applications

Creating and Comparing Sets of Principal Component Images 279
F. Pedersen

General-Purpose Soft Tissue Segmentation from Medical Images 293
I. Carlbom, T. Kapur, G. Klinker, D. Terzopoulos, and L. Thurfjell

Measuring Shape and Motion of White Blood Cells from Sequences of Fluorescence Microscopy Images 305
L. Yang, F. Albregtsen, T. Lønnestad, P. Grøttum, J.-G. Iversen, J. S. Røtnes and J-A. Røttingen

Mapping the Human Retina 317
A. Pinz, M. Prantl and P. Datlinger

Restoration of Radial Optical Flows in Echocardiographic Sequences 331
L. Floreby and G. Salomonsson

Initial Results of Automated Melanoma Recognition 343
H. Ganster, M. Gelautz, A. Pinz, M. Binder, H. Pehamberger, M. Bammer and J. Krocza

Industrial Applications

Near-Sensor Real Time Spectral Classification for Industrial Applications 355
E. Åstrand, M. Österberg, O. Hagman and A. Åström

A Color Vision Approach for Grading Lumber 367
H. Kauppinen and O. Silvén

Automatic Fruit Blemish Detection 381
Q.-S. Yang

On Edge Density for Automatic Size Inspection 393
W.-X. Wang and F. Bergholm

MODELLING AND TESTING THE STABILITY OF EDGE SEGMENTS: LENGTH AND ORIENTATION

Claus B. Madsen, Henrik I. Christensen
Aalborg University
Fr. Bajers Vej 7D, DK–9220 Aalborg Ø, Denmark
e-mail: [cbm, hic]@vision.auc.dk

Abstract

This paper derives a model for the variance in the length and orientation of edge segments extracted from an image. It is assumed that edge pixel positions are subject to noise. The effect of this positional uncertainty is propagated all the way to segment length and orientation. The model predicts an approximately constant variance in segment length, whereas the variance in segment orientation decreases with increased segment length.

The theoretical model is verified by experiments on real images and it is shown that segment orientation is more stable (has higher signal to noise ratio) than length for segments longer than 1/10 of the image size.

1 Introduction

Edge segments extracted from images is one of the most widely used (intermediate) representations in computer vision. Edge segments are used statically for recognition and/or pose estimation from single intensity images. Dynamically, edge segments are used for as diverse purposes as structure from motion, (e.g., [8]) and control of camera motion, (e.g., [6, 9]).

While being very common in computer vision, edge segments have not been studied extensively in terms of stability. This paper addresses this issue by investigating a model for the variance in the length and the orientation of an edge segment fitted to a noisy population of edge pixels.

Obviously, modelling the noise on image derived features is a very complex matter indeed. So many parameters are involved in the imaging process, (lighting, scene contents, equipment, parameters of algorithms etc.), that it is virtually impossible to include them all into a model. This has mostly led to researchers either not addressing the problem of stability of their algorithms towards instability in edge

segments, or at best algorithms are being tested with synthetically generated edge segments perturbed with Gaussian noise of known variance.

Few references contain useful information on the expected noise level on line segment lengths and orientation. [5, 4] argue, that line segment length is inherently unreliable and base their pose estimation method solely on 'infinite' image lines determined by the position, (distance to origin), of each segment and its orientation. They test their approach for noise sensitivity using orientation noise levels of 1° and 5°, (standard deviation), respectively. They do not relate these noise levels to any experimentally obtained variances.

In an interesting paper, ([7]), the sensitivity of a pose estimation technique is modelled as a function of edge segment orientation uncertainty. The paper assumes a 5 degree error on orientations of edge segments, ($\pm$ measure). Again, this work does not present any experimentally obtained values.

The few above mentioned works represent typical ways of dealing with the problem of noise in extracted edge segments. Some theoretical work on the problem can be found in [3, 2, 1]. [3] and [2] derives covariance matrices for the parameters of infinite straight lines fitted to edge pixels, e.g., the a and b parameters in a $u + av + b = 0$ representation.

The work described in [1] addresses uncertainty problems for trinocular stereo, and does it via uncertainty on edge segment endpoints. The paper describes the transformation of a Gaussian edge pixel noise model to a covariance matrix for the coordinates of edge segment endpoints.

None of the cited works compare the theoretical considerations to noise estimations from experiments on real images. I.e., they provide no parameterization in terms of variances determined from repeatedly imaging the same scene.

This paper extends the segment endpoint uncertainty analysis presented in [1] by presenting the derivation of a orientation/length covariance matrix and the model is parameterized with experiments on real images. Sections 2 and 3 briefly summarize the results from [1]; section 4 then demonstrates how to express a model for the uncertainty in segment length and orientation due to edge pixel noise, and finally, experiments are presented that demonstrate the most important aspects of the theoretical model.

2 From edgels to an edge segment

Consider a set of paired measurements $(x_i, y_i), i = 1...n$ corresponding to the coordinates of n edge pixels as found by some edge detection process. Assume that both x and y are subject to error. Deriche et al. adopt the representation of an infinite straight line given in Eq. (1). They then demonstrate how the parameters τ and ρ can be computed from the first and second order moments of the edge pixel population to provide a least squares fit:

$$x \sin(\tau) - y \cos(\tau) + \rho \;=\; 0 \qquad (1)$$

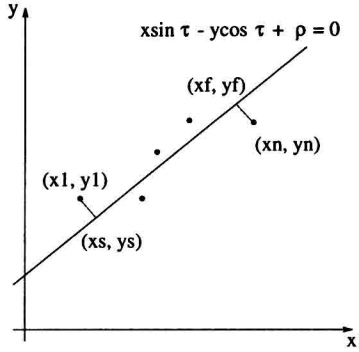

Figure 1: Fitting an edge segment to a string of edge pixels.

where

$$\bar{x} = \frac{1}{n}\sum_{i=1}^{n} x_i \qquad \bar{y} = \frac{1}{n}\sum_{i=1}^{n} y_i$$

$$a = \sum_{i=1}^{n}(x_i - \bar{x})^2 \qquad b = 2\sum_{i=1}^{n}(x_i - \bar{x})(y_i - \bar{y}) \qquad c = \sum_{i=1}^{n}(y_i - \bar{y})^2$$

$$\tau = \frac{1}{2}\arctan\left(\frac{b}{a-c}\right) \tag{2}$$

$$\rho = \bar{y}\cos(\tau) - \bar{x}\sin(\tau) \tag{3}$$

Having fitted an infinite straight line to a population of edge pixels, a line segment can be defined by projecting the extent of the population onto the fitted line. Assuming the original edge pixel population is ordered this can be achieved by projection of the first and the last pixel, (see figure 1). If $P_s(x_s, y_s)$ and $P_f(x_f, y_f)$ denote the start and finish endpoint of the segment respectively:

$$x_s = x_1 - (x_1\sin(\tau) - y_1\cos(\tau) + \rho)\sin(\tau) \tag{4}$$

$$y_s = y_1 + (x_1\sin(\tau) - y_1\cos(\tau) + \rho)\cos(\tau) \tag{5}$$

$$x_f = x_n - (x_n\sin(\tau) - y_n\cos(\tau) + \rho)\sin(\tau) \tag{6}$$

$$y_f = y_n + (x_n\sin(\tau) - y_n\cos(\tau) + \rho)\cos(\tau) \tag{7}$$

3 Covariance of edge segment end points

The infinite straight line fit by the moments is a least square error fit if the two coordinates of edge pixels have the same variance. Thus, if Σ is the covariance matrix

associated with each edge pixel, and σ_{pixel} is the standard deviation of the edge pixel coordinate noise distribution:

$$\Sigma = \begin{bmatrix} \sigma^2_{pixel} & 0 \\ 0 & \sigma^2_{pixel} \end{bmatrix} \tag{8}$$

Arguably, a non-isotropic noise model could be assumed, with different variances for each coordinate, i.e., σ^2_{xx} and σ^2_{yy}. Only, if they are not the same, the fit is no longer a least mean square error fit.

Assuming the basic edge pixel noise model represented by Eq. (8), it is possible to compute the covariance matrices of different parameters of the final segment. It can be shown, that the covariance matrix of the parameters of the infinite line, (τ and ρ), becomes:

$$\Lambda = \frac{(a+c)\sigma^2_{pixel}}{(a-c)^2+b^2} \begin{bmatrix} 1 & -d \\ -d & d^2 \end{bmatrix} + \begin{bmatrix} 0 & 0 \\ 0 & \frac{\sigma^2_{pixel}}{n} \end{bmatrix} \tag{9}$$

$$d = \bar{y}\sin(\tau) + \bar{x}\cos(\tau) \tag{10}$$

The coordinate covariance matrices of the two segment endpoints can be computed using the relations in Eqs. (4) through (7). Using the start endpoint as example, the vector $\vec{v}_s = [\ x_s \quad y_s\ ]$ expresses the endpoint coordinates as functions of the coordinates of a vector $\vec{p}_1 = [\ \tau \quad \rho \quad x_1 \quad y_1\ ]$. If Δ^s is the covariance matrix associated with the coordinates of the endpoint:

$$\Delta^s = \begin{bmatrix} \sigma^2_{x_s x_s} & \sigma^2_{x_s y_s} \\ \sigma^2_{x_s y_s} & \sigma^2_{y_s y_s} \end{bmatrix} = \frac{\partial \vec{v}_s}{\partial \vec{p}_1} \Gamma \frac{\partial \vec{v}_s}{\partial \vec{p}_1}^T \tag{11}$$

where $\partial\vec{v}_s/\partial\vec{p}_1$ is the 2×4 Jacobian matrix and Γ is the 4×4 covariance of $\vec{p}_1$:

$$\Gamma = \begin{bmatrix} & & 0 & 0 \\ & \Lambda & & \\ & & 0 & 0 \\ 0 & 0 & & \\ & & & \Sigma \\ 0 & 0 & & \end{bmatrix} \tag{12}$$

Thus, Δ^s is a 2×2 covariance matrix expressing the two variances of the 2D distribution function of endpoint coordinates. From the eigenvectors of the covariance matrix, the directions of maximum and minimum variance can be found.

4 Covariance of edge segment length and orientation

It is generally accepted that edge segment orientation is more stable than length. While the covariance matrices of the two endpoints are useful for many purposes, it

is equally important to study the uncertainties of orientation and length due to edge pixel position noise.

In order to be able to compare the variances in orientation and length signal-to-noise ratios can be studied or, equivalently, the orientation and length variables can be normalized against the respective maximum attainable values. For this study the latter approach has been chosen since it results in a more versatile formulation in terms of interpreting information from the covariance matrix.

The orientation of an edge segment has a dynamic range of π, (is modulo π), thus the maximum attainable value can be said to be $\tau_{max} = \pi$. The maximum length of an edge segment is $l_{max} = 512$ if the segment is to fall entirely within the image for any orientation, (and assuming all coordinates are in pixels). By normalizing orientation and length with these two maximum values we obtain two stochastic variables with dynamic ranges $]-0.5; 0.5[$ and $[0; 1]$ respectively:

$$\tau = (1/\tau_{max}) \arctan\left(\frac{y_f - y_s}{x_f - x_s}\right) \tag{13}$$

$$l = (1/l_{max})\sqrt{(x_f - x_s)^2 + (y_f - y_s)^2} \tag{14}$$

If we assign the coordinates of a vector $\vec{F} = [\tau, l]^T$ and $\vec{G} = [x_s, y_s, x_f, y_f]$, then the covariance $\Xi^{\tau l}$ of the vector $\vec{F}$ can be expressed as:

$$\Xi^{\tau l} = \frac{\partial \vec{F}}{\partial \vec{G}} \Upsilon \frac{\partial \vec{F}^T}{\partial \vec{G}} \tag{15}$$

where $\partial\vec{F}/\partial\vec{G}$ is the 2×4 Jacobian matrix of the orientation and length functions, and Υ is the 4×4 covariance matrix of $\vec{G}$, i.e., the endpoints. Eq. (15) expresses a first order approximation to the covariance matrix. In numerical examples we have probed the size of the second order terms against the first order terms in a Taylor expansion of both τ and l and found the second order terms to be at least two orders of magnitude smaller than the first order terms.

It can be proved, ([1]), that the correlation between one endpoint and the τ and ρ parameters of the fitted infinite line is inversely proportional to the number of edge pixels in the population. From this we justify, that zero correlation between endpoints can be assumed, and thus:

$$\Upsilon = \begin{bmatrix} & & 0 & 0 \\ & \Delta^s & & \\ & & 0 & 0 \\ 0 & & & \\ & 0 & & \Delta^f \\ 0 & & & \end{bmatrix} \tag{16}$$

The Δ^s and Δ^f are computed from Eq. (11) using appropriate changes of indices for the latter of the two matrices, (the finish endpoint).

Using ordinary partial differentiation we get the elements of the Jacobian matrix of the mappings from segment endpoints to orientation and length:

$$\frac{\partial \vec{F}}{\partial \vec{G}} = \begin{bmatrix} \frac{\partial \tau}{\partial x_s} & \frac{\partial \tau}{\partial y_s} & \frac{\partial \tau}{\partial x_f} & \frac{\partial \tau}{\partial y_f} \\ \frac{\partial l}{\partial x_s} & \frac{\partial l}{\partial y_s} & \frac{\partial l}{\partial x_f} & \frac{\partial l}{\partial y_f} \end{bmatrix}$$

$$\frac{\partial \tau}{\partial x_s} = \frac{1}{\tau_{max}} \frac{y_f - y_s}{l_{max}^2 l^2} \qquad \frac{\partial \tau}{\partial y_s} = \frac{-1}{\tau_{max}} \frac{x_f - x_s}{l_{max}^2 l^2} \qquad \frac{\partial \tau}{\partial x_f} = \frac{-1}{\tau_{max}} \frac{y_f - y_s}{l_{max}^2 l^2} \qquad \frac{\partial \tau}{\partial y_f} = \frac{1}{\tau_{max}} \frac{x_f - x_s}{l_{max}^2 l^2}$$

$$\frac{\partial l}{\partial x_s} = \frac{-1}{l_{max}} \frac{x_f - x_s}{l_{max} l} \qquad \frac{\partial l}{\partial y_s} = \frac{-1}{l_{max}} \frac{y_f - y_s}{l_{max} l} \qquad \frac{\partial l}{\partial x_f} = \frac{1}{l_{max}} \frac{x_f - x_s}{l_{max} l} \qquad \frac{\partial l}{\partial y_f} = \frac{1}{l_{max}} \frac{y_f - y_s}{l_{max} l}$$

Evidently, there is a high degree of symmetry in the individual Jacobian matrix elements (apart from signs). We can therefore write the matrix as:

$$\frac{\partial \vec{F}}{\partial \vec{G}} = \begin{bmatrix} \frac{\partial \tau}{\partial x_s} & \frac{\partial \tau}{\partial y_s} & \frac{-\partial \tau}{\partial x_s} & \frac{-\partial \tau}{\partial y_s} \\ \frac{\partial l}{\partial x_s} & \frac{\partial l}{\partial y_s} & \frac{-\partial l}{\partial x_s} & \frac{-\partial l}{\partial y_s} \end{bmatrix}$$

4.1 Qualitative observations

All information required to compute the covariance matrix from Eq. (15) is present. Unfortunately, writing out the covariance matrix yields rather complex expressions. In the numerical examples below the correct approach has been used, but in favor of a behavioural characteristic an assumption shall be adopted.

The following can be noted about the covariance matrix, Υ, of the two endpoints: 1) all elements in Υ stem from the two covariance matrices Δ^s and Δ^f of the endpoints,- these are symmetric matrices and 2) the covariance matrix of the start endpoint can approximately be said to equal that of the other endpoint. Using this latter assumption:

$$\Upsilon = \begin{bmatrix} \sigma_{x_s x_s}^2 & \sigma_{x_s y_s}^2 & 0 & 0 \\ \sigma_{x_s y_s}^2 & \sigma_{y_s y_s}^2 & 0 & 0 \\ 0 & 0 & \sigma_{x_s x_s}^2 & \sigma_{x_s y_s}^2 \\ 0 & 0 & \sigma_{x_s y_s}^2 & \sigma_{y_s y_s}^2 \end{bmatrix} \tag{17}$$

It is now possible to compute a tractable expression for the covariance between orientation and length. From Eq. (15):

$$\begin{aligned} \Xi^{\tau l} &= \begin{bmatrix} \frac{\partial \tau}{\partial x_s} & \frac{\partial \tau}{\partial y_s} & \frac{-\partial \tau}{\partial x_s} & \frac{-\partial \tau}{\partial y_s} \\ \frac{\partial l}{\partial x_s} & \frac{\partial l}{\partial y_s} & \frac{-\partial l}{\partial x_s} & \frac{-\partial l}{\partial y_s} \end{bmatrix} \begin{bmatrix} \sigma_{x_s x_s}^2 & \sigma_{x_s y_s}^2 & 0 & 0 \\ \sigma_{x_s y_s}^2 & \sigma_{y_s y_s}^2 & 0 & 0 \\ 0 & 0 & \sigma_{x_s x_s}^2 & \sigma_{x_s y_s}^2 \\ 0 & 0 & \sigma_{x_s y_s}^2 & \sigma_{y_s y_s}^2 \end{bmatrix} \begin{bmatrix} \frac{\partial \tau}{\partial x_s} & \frac{\partial l}{\partial x_s} \\ \frac{\partial \tau}{\partial y_s} & \frac{\partial l}{\partial y_s} \\ \frac{-\partial \tau}{\partial x_s} & \frac{-\partial l}{\partial x_s} \\ \frac{-\partial \tau}{\partial y_s} & \frac{-\partial l}{\partial y_s} \end{bmatrix} \\ &= \begin{bmatrix} \sigma_{\tau\tau}^2 & \sigma_{\tau l}^2 \\ \sigma_{\tau l}^2 & \sigma_{ll}^2 \end{bmatrix} \end{aligned} \tag{18}$$